Wall-boundary conditions in probability density function methods and application to a turbulent channel flow

Jean-Pierre Minier
Laboratoire National d'Hydraulique, Electricité de France, 6 Quai Watier, 78400 Chatou, France

Jacek Pozorski
Instytut Maszyn Przeplywowych, Polska Akademia Nauk, ul. Fiszera 14, 80952 Gdańsk, Poland

(Received 2 September 1998; accepted 24 May 1999)

An application of a probability density function (PDF), or Lagrangian stochastic, approach to the case of high-Reynolds number wall-bounded turbulent flows is presented. The model simulates the instantaneous velocity and dissipation rate attached to a large number of particles and the wall-boundary conditions are formulated directly in terms of the particle properties. The present conditions aim at reproducing statistical results of the logarithmic region and are therefore in the spirit of wall functions. A new derivation of these boundary conditions and a discussion of the resulting behavior for different mean variables, such as the Reynolds stress components, is proposed. Thus, the present paper complements the work of Dreeben and Pope [Phys. Fluids **9**, 2692 (1997)] who proposed similar wall-boundary particle conditions. Numerical implementation of these conditions in a standalone two-dimensional PDF code and a pressure-correction algorithm are detailed. Moments up to the fourth order are presented for a high-Reynolds number channel flow and are analyzed. This case helps to clarify how the method works in practice, to validate the boundary conditions and to assess the model and the code performance. © *1999 American Institute of Physics.* [S1070-6631(99)01209-X]

I. INTRODUCTION

Most turbulence models try to express the equations satisfied by the mean variables of interest (for example, the ensemble averaged or filtered velocity) by applying directly the averaging operator (be it Reynolds averaging or spatial filtering) to the Navier–Stokes equations and assuming some constitutive relations. Classical models consist therefore in an Eulerian description and a set of partial differential equations (PDEs). Numerous results, related for instance to near-wall behavior, are often expressed within that Eulerian framework. In contrast, (Lagrangian) probability density function (PDF) methods are formulated in terms of particles and of stochastic differential equations (SDEs).[1–8] Broadly speaking, PDF models can be regarded as an intermediate level of description between the exact (microscopic) dynamics and the (macroscopic) dynamics of the mean statistical variables of interest. They provide ''underlying'' information with respect to the chosen macroscopic variables. PDF models can be used to reconstitute subgrid information or fluctuations in LES modeling,[4] or simply instantaneous one-point fluctuations in Reynolds-stress modeling. They are therefore particularly interesting when such extra information is needed. One such example is for reactive flows where source terms, however complicated and nonlinear, are treated without approximation by PDF models while they remain nearly intractable at the macroscopic level.[1,5] Another example is two-phase flows where variations in particle properties pose a similar challenge.[3,6] PDF models have also an interest for constant-density flows. Since convection is treated without approximation, there is no need of a gradient-diffusion hypothesis in particular for the triple velocity correlation. Furthermore, PDF methods can easily take into account internal intermittency and can also model external intermittency in a straightforward way.[7] In the PDF framework, there is an infinite hierarchy of PDF models[8] each of which defines the information that is available (one-point, two-point,... PDFs). One-point PDFs provide only one-point information but are, at the moment, more developed than two-point PDF models especially for the general case of nonstationary nonhomogeneous turbulence.

In this paper, we limit ourselves to present state-of-the-art one-point PDF models (also called one-particle Lagrangian models) that we wish to use for general flows. Simulations of these flows require appropriate boundary conditions to be formulated in terms of the particle properties, that is within the PDF framework. The purpose of this paper is to present particle boundary conditions that aim at reproducing the momentum exchange between the wall and the bulk of the flow. The objective is not to simulate the boundary layer down to the viscous layer and to the no-slip condition but precisely to avoid computing this highly nonhomogeneous and thin region by bridging over it. In other words, we are looking for the equivalent of the so-called ''wall functions'' in classical turbulence models. Representing the real and complete boundary layer and near-wall fluid phenomena in detail would be preferable. However, the present choice of a wall-function treatment is made for several reasons. First, it is simpler and less computationally demanding since it avoids the explicit treatment of the high-gradient zone. It appears as a reasonable first step towards a full treatment of

the boundary layer. Second, it is also justified if the objective of a simulation is focused on the bulk of the flow and if one simply wants a macroscopic way to represent the effect of walls. Third, present PDF models are developed for high-Reynolds flows and limiting ourselves to the logarithmic region is therefore consistent with assumptions made to derive the model. A near-wall treatment requires the explicit modeling of molecular viscosity effects and the use of a different model.[9,10] One modification is the appearance of a white-noise term, expressing Brownian motion, in the particle location equation. As a consequence, the general set of SDEs of the extended model is of a different form and writing an accurate numerical scheme[11] is more difficult.[12]

A wall-function treatment in terms of particles has first been proposed by Pope and incorporated in the PDF computation;[13] it is further developed and detailed in Dreeben and Pope.[14] Similar conditions will be used here. However, the purpose of this paper is to put forward an alternative derivation of the particle boundary conditions. Another condition for particle frequency is discussed and resulting conditions for various mean variables, such as Reynolds-stress components, are reported. This is believed to complement the work of Dreeben and Pope. Another purpose is to present the derivation of the mean equations, and their equilibrium values in the constant-stress layer, only through a particle stochastic point of view by manipulating directly the governing SDEs. Also for reason of completeness, numerical results are presented for a high-Reynolds number channel flow and are compared to the experimental measurements of Comte-Bellot.[15] These results have been obtained with a simple PDF model but from a full two-dimensional standalone particle simulation. The aim of the present computations is not to obtain the best possible results but rather to illustrate how the general method works for a given case and also to bring out a number of numerical issues.

This paper is organized as follows. The Lagrangian stochastic model used is briefly presented in Sec. II. The main assumptions behind the model and that are useful for later considerations are recalled and the corresponding mean equations are written. Boundary conditions are developed in Sec. III. Basic facts of a general numerical algorithm are presented in Sec. IV and results for the channel flow case are discussed in Sec. V.

II. STOCHASTIC MODELING

In the following, we limit ourselves to one-point PDF models for incompressible flows. The models considered have been developed mostly by Pope and co-workers[16–18] and a number of reviews provide details on the construction of the models and on their physical justification.[2,3,5] The purpose of this section is therefore simply to present the salient features of the model that will be useful for later derivations.

A. Lagrangian stochastic model

There are several ways to present a PDF model. Here, we adopt right from the outset a Lagrangian point of view. The starting point are the instantaneous evolution equations for variables describing the fluid motion in the Lagrangian formulation (a ''+'' sign denotes values taken along a particle trajectory):

$$d\mathbf{x}^+ = \mathbf{U}^+ dt, \tag{1}$$

$$d\mathbf{U}^+ = \left(-\frac{1}{\rho}\frac{\partial P}{\partial \mathbf{x}} + \nu \Delta \mathbf{U} \right)^+ dt. \tag{2}$$

Reynolds averaging is applied to decompose variables, like the Eulerian velocity $\mathbf{U}$ and pressure P fields, into mean and fluctuating parts

$$U_i = \langle U_i \rangle + u_i, \quad P = \langle P \rangle + p. \tag{3}$$

In the one-point PDF approach, the fluctuating terms which are functions of the instantaneous fields are unknown and have to be modeled. The main idea is to replace the exact instantaneous equations by modeled but still instantaneous equations

$$dx_i^+ = U_i^+ dt, \tag{4}$$

$$dU_i^+ = -\frac{1}{\rho}\frac{\partial \langle P \rangle}{\partial x_i} dt + G_{ij}(U_j^+ - \langle U_j \rangle) dt + \sqrt{C_0 \langle \epsilon \rangle}\, dW_i, \tag{5}$$

where dW_i is the increment of an isotropic Wiener process $\mathbf{W}$.[19,20] The mean terms on the rhs of Eq. (5) are to be regarded as the value of the corresponding mean field taken at the particle location at time t. We are now dealing with a stochastic process and with the SDEs that constitute the time evolution equations of the trajectories of the process, here made up by the joint particle location and velocity variables $\mathbf{Y} = (\mathbf{x}^+, \mathbf{U}^+)$. The stochastic process used to model fluid particle velocity is a diffusion process.[19] The form of the model can be assumed beforehand and justified by its relations with Reynolds-stress modeling or, alternatively, can be derived from underlying principles using Onsager's hypotheses.[21] Indeed, various choices can be made for the drift (by assuming different constitutive relations for the matrix G_{ij}) and diffusion coefficients, resulting in different mean Reynolds-stress equations.[22] Here, we limit ourselves to the simple Langevin model (SLM) where G_{ij} assumes an isotropic form with a single timescale expressed as a function of $k/\langle \epsilon \rangle$, k being the fluid kinetic energy $k = 0.5\langle u_i u_i \rangle$ and $\langle \epsilon \rangle$ its mean dissipation rate

$$G_{ij} = -\left(\frac{1}{2} + \frac{3}{4} C_0 \right) \frac{\langle \epsilon \rangle}{k} \delta_{ij}. \tag{6}$$

For the model to be self-contained, the values of the mean dissipation rate at the particle locations must be known. This can be done by writing a PDE for $\langle \epsilon \rangle$ or, in a way consistent with the present stochastic approach explained in the Introduction, by actually writing a model for the instantaneous dissipation rate along particle paths, namely $\epsilon^+ = \epsilon(t, \mathbf{x}^+)$. Including this information not only gives access to the mean value but also allows internal and external intermittency to be directly simulated.[7] In this paper, the evolution equation for the instantaneous turbulent energy dissipation rate is built upon the refined Kolmogorov hypoth-

esis which states that ϵ is a lognormally-distributed random variable. The equation is developed not in terms of the dissipation itself but rather in terms of the turbulent frequency[17] or relaxation rate. The Eulerian mean turbulent frequency field can be defined as

$$\langle \omega \rangle = \frac{\langle \epsilon \rangle}{k}. \tag{7}$$

In the approach followed here, the required mean values are extracted from the particle simulation by solving an equation for a particle property ω^+. This Lagrangian quantity appears as an instantaneous turbulent frequency and can be seen as

$$\omega^+ = \frac{\epsilon^+}{k}. \tag{8}$$

The modeled Lagrangian ω equation has the form[18]

$$d\omega^+ = -\omega^+ \langle \omega \rangle S_\omega dt - \omega^+ \langle \omega \rangle C_\chi \left[\ln\left(\frac{\omega^+}{\langle \omega \rangle} \right) - \left\langle \frac{\omega}{\langle \omega \rangle} \ln\left(\frac{\omega}{\langle \omega \rangle} \right) \right\rangle \right] dt + \omega^+ \sqrt{2 C_\chi \langle \omega \rangle \sigma^2}\, dW. \tag{9}$$

The starting point is to assume that $\chi^+ = \ln(\omega^+/\langle \omega \rangle)$ is a normally-distributed variable and that it can be represented by a simple Ornstein–Uhlenbeck process. In Eq. (9), σ^2 is the variance of χ and C_χ is a constant. The equation for ω^+ has been modeled so that the evolution of $\langle \omega \rangle$ agrees with the standard form known from the $k-\epsilon$ turbulence model in homogeneous turbulence. S_ω stands for the normalized decay rate of $\langle \omega \rangle$ and is modeled by reference to the standard equation of $\langle \epsilon \rangle$ using constants $C_{\epsilon 1}$ and $C_{\epsilon 2}$:

$$S_\omega = (C_{\epsilon 2} - 1) - (C_{\epsilon 1} - 1) \frac{\mathcal{P}}{\langle \epsilon \rangle}, \tag{10}$$

where $\mathcal{P}$ is the turbulent kinetic energy production term

$$\mathcal{P} = -\langle u_i u_k \rangle \frac{\partial \langle U_i \rangle}{\partial x_k}. \tag{11}$$

It should be noted that since the mean velocity gradients and the Reynolds stresses can be directly obtained from particles properties, the production term $\mathcal{P}$ is simply computed using the above equation, Eq. (11) and not from its expression in the k-ϵ model as used in other works[17,18]

$$\frac{\mathcal{P}}{\langle \epsilon \rangle} = 2 C_\mu \frac{S_{ij} S_{ij}}{\langle \omega \rangle^2}. \tag{12}$$

Apart from being the exact expression, the first form, Eq. (11), appears as less noisy in the computations and is therefore chosen. Another model has been proposed recently for the frequency[23] and used by Dreeben and Pope[14] where the limit distribution in homogeneous turbulence is not a lognormal but a gamma distribution. However, the lognormal model which is based on a clear and physical assumption,[24] although it is still debated, has been preferred and retained in this work.

Broadly speaking, the Lagrangian stochastic (or one-point PDF) model consists in simulating a large number of particles. Variables are attached to each particle and follow time evolution equations. The particles interact only indirectly by first creating mean fields, such as $\langle \mathbf{U} \rangle$, which are then applied to each particle (it is a mean-field approach). Generally, the above set of equations can be thought of as describing a vector stochastic diffusion process and can be written

$$d\mathbf{Y} = \mathbf{D}(t, \mathbf{Y}) dt + B(t, \mathbf{Y}) d\mathbf{W}. \tag{13}$$

$\mathbf{Y}$ stands for the vector of the state variables which have been chosen, $\mathbf{D}$ and $B = (B_{ij})$ denote, respectively, the drift vector and the diffusion matrix. In the present case, the vector of state variables gathers particle location, velocity and frequency $\mathbf{Y} = (x^+, \mathbf{U}^+, \omega^+)$. It is important to note basic properties of the present model. In homogeneous turbulence the different coefficients entering the SDEs are constant: the drift is linear and the diffusion coefficient is constant. As a result, the one-point velocity PDF is Gaussian in agreement with experimental findings. Furthermore, in that case the complete vector of state variables, $(\mathbf{U}^+, \ln(\omega^+))$ forms a joint-normal distribution.

B. Mean equations

From the closed instantaneous evolution equations, Eqs. (4), (5), and (9), or in general form Eq. (13), a corresponding PDF equation can be derived. Since the vector of state variables is modeled by a diffusion process, the equation satisfied by the Lagrangian PDF $f(t,y)$, where $\mathbf{y} = (\mathbf{x}, \mathbf{V}, \mathbf{\Omega})$ is the the sample space variable, is a Fokker–Planck equation[19,20]

$$\frac{\partial f}{\partial t} = -\frac{\partial [D_i f]}{\partial y_i} + \frac{1}{2} \frac{\partial^2 [(BB^\perp)_{ij} f]}{\partial y_i \partial y_j}, \tag{14}$$

where $B^\perp$ is the transpose of B. In the present approach, an incompressible turbulent flow is represented by an ensemble of fluid particles each of the same small mass. From the set of particles, various Lagrangian or Eulerian statistics can be extracted. An Eulerian average is taken at a fixed point in space $\mathbf{x}$ and at a fixed time t, and the Eulerian PDF corresponds to the Lagrangian PDF conditioned on the particle position. Thus, for a fluid property function of the velocity and turbulent frequency fields $Q(t,\mathbf{x}) = Q(t, \mathbf{U}(t,\mathbf{x}), \omega(t,\mathbf{x}))$, the correspondence between Lagrangian and Eulerian averages is expressed by

$$\langle Q(t, \mathbf{x}^+, \mathbf{U}^+, \omega^+) | \mathbf{x}^+ = x \rangle = \langle Q(t, \mathbf{x}) \rangle. \tag{15}$$

The usual way to derive the desired mean equations is to express the equation satisfied by the Eulerian PDF and to integrate that equation after multiplication by the proper variable. Pursuing our trajectory point of view, the mean equations are derived here directly from the SDEs by applying the rules of stochastic calculus.

In the PDF point of view, the normalization condition of f yields immediately the zero divergence equation. There is a direct relation between a correct mean pressure gradient ($\langle P \rangle$ is the solution of the ''correct'' Poisson equation) and the PDF normalization condition.[1] Indeed, for a particle system, each of which represents the same amount of mass, to be an acceptable representation of the flow, it is required that the particle position PDF be proportional to the fluid density.

Since we are dealing with incompressible flows, this means that particles must be uniformly distributed in the domain. In the particle simulations, the condition of mass conservation is directly enforced by calculating the mean pressure gradient for that purpose (see Sec. IV). Therefore, by construction, we have for the Eulerian mean velocity field

$$\frac{\partial \langle U_i \rangle}{\partial x_i} = 0. \tag{16}$$

The mean momentum equation is simply obtained by applying the averaging operator to the particle velocity equation (5):

$$\langle dU_i^+ | \mathbf{x}^+ = x \rangle = -\frac{1}{\rho}\frac{\partial \langle P \rangle}{\partial x_i} dt. \tag{17}$$

Using the relation between the instantaneous substantial derivative and its Eulerian counterpart

$$\frac{d}{dt} = \frac{\partial}{\partial t} + U_j \frac{\partial}{\partial x_j}, \tag{18}$$

we obtain

$$\frac{\partial \langle U_i \rangle}{\partial t} + \langle U_j \rangle \frac{\partial \langle U_i \rangle}{\partial x_j} + \frac{\partial \langle u_i u_j \rangle}{\partial x_j} = -\frac{1}{\rho}\frac{\partial \langle P \rangle}{\partial x_i}. \tag{19}$$

Thus, the high-Reynolds form of the mean Navier–Stokes equation is satisfied.

To obtain the second-order equations, the instantaneous equation for the fluctuating velocity components along a particle trajectory is expressed using

$$\begin{aligned} \frac{du_i^+}{dt} &= \frac{dU_i^+}{dt} - \frac{d\langle U_i \rangle}{dt} \\ &= \frac{dU_i^+}{dt} - \left\{ \frac{\partial \langle U_i \rangle}{\partial t} + \langle U_j \rangle \frac{\partial \langle U_i \rangle}{\partial x_j} \right\} - u_j^+ \frac{\partial \langle U_i \rangle}{\partial x_j}. \end{aligned} \tag{20}$$

The equation is written in an incremental form to properly handle the stochastic terms and with the mean Navier–Stokes equation, we get

$$\begin{aligned} du_i^+ = &-\frac{\partial \langle u_i u_k \rangle}{\partial x_k} dt - u_k^+ \frac{\partial \langle U_i \rangle}{\partial x_k} dt + G_{ik} u_k^+ \, dt \\ &+ \sqrt{C_0 \langle \epsilon \rangle} dW_i. \end{aligned} \tag{21}$$

The different SDEs are defined in the Ito sense and the derivatives of the products $u_i u_j$ are obtained from Ito's formula[19,20]

$$d(u_i^+ u_j^+) = u_i^+ \, du_j^+ + u_j^+ \, du_i^+ + C_0 \langle \epsilon \rangle dt \, \delta_{ij}. \tag{22}$$

The mean second-order equations are then

$$\begin{aligned} &\frac{\partial \langle u_i u_j \rangle}{\partial t} + \langle U_k \rangle \frac{\partial \langle u_i u_j \rangle}{\partial x_k} + \frac{\partial \langle u_i u_j u_k \rangle}{\partial x_k} \\ &= -\langle u_i u_k \rangle \frac{\partial \langle U_j \rangle}{\partial x_k} - \langle u_j u_k \rangle \frac{\partial \langle U_i \rangle}{\partial x_k} + G_{ik} \langle u_j u_k \rangle \\ &\quad + G_{jk} \langle u_i u_k \rangle + C_0 \langle g e \rangle \delta_{ij}. \end{aligned} \tag{23}$$

Thus, the SLM model corresponds to the Rotta model for the transport equations of $\langle u_i u_j \rangle$.

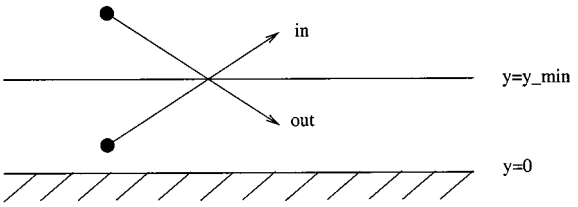

FIG. 1. Particle boundary conditions applied at the surface $y = y_{\min}$ located in the logarithmic layer.

The equation for the mean $\langle \omega \rangle$, derived from Eq. (9), takes the form

$$\left\langle \frac{d\omega}{dt} \right\rangle = \frac{\partial \langle \omega \rangle}{\partial t} + \langle U_i \rangle \frac{\partial \langle \omega \rangle}{\partial x_i} + \frac{\partial}{\partial x_i} \langle u_i \omega \rangle = -\langle \omega \rangle^2 S_\omega. \tag{24}$$

III. BOUNDARY CONDITIONS

A. Conditions for instantaneous variables

The presence of the wall is taken into account by formulating the conditions for the boundary of the computational domain, placed at $y_{\min}$ in the constant-stress region of the turbulent boundary layer, the so-called logarithmic layer, see Fig. 1. From here onwards, we use x, y and z to represent the longitudinal, normal and spanwise coordinates. Correspondingly, the velocity components are expressed as u, v and w. The important parameter that represents the effect of wall proximity is the friction velocity $u_* = \sqrt{\tau_w / \rho}$, where τ_w is the wall shear stress. Variations of mean variables in the constant-stress region are well known

$$\langle uv \rangle = -u_*^2, \quad \mathcal{P} = \langle \epsilon \rangle = \frac{u_*^3}{\kappa y}, \quad \frac{\partial \langle U \rangle}{\partial y} = \frac{u_*}{\kappa y}. \tag{25}$$

In the PDF approach, the boundary conditions must be applied to the instantaneous variables attached to the particles, as shown in Fig. 1. Every time a particle crosses the boundary and gets out of the domain, it is reflected back into it, to ensure zero net mass flux. The simplest condition on the velocity component normal to the wall of any particle leaving the domain is

$$V_{\text{in}}^+ = -V_{\text{out}}^+. \tag{26}$$

This gives in the mean $\langle V \rangle_b = 0$ where $\langle \cdot \rangle_b$ denotes the ensemble average over the flux of particles that cross the domain boundary.

The desired condition for the particle longitudinal velocity is slightly more involved. Indeed, the issue is to write the instantaneous axial velocity U_{in} of the incoming (reflected) particle in terms of the velocity of the outgoing one. One cannot simply equate the two since it would mean that there is no momentum exchange with the wall whereas this is precisely what we want to reproduce. In the Dreeben and Pope[14] formulation of the wall-boundary conditions in the particle approach, it was supposed that the velocity component parallel to the wall obeys

$$U_{\text{in}}^+ = U_{\text{out}}^+ + \alpha V_{\text{out}}^+$$

and α was then deduced using a formula for the flux. That presentation remains in the spirit of the Reynolds stress closure: one supposes a formula first and finds values of the constants appearing in it from some macroscopic constraints (i.e., given fluxes).

Here, a different formulation is proposed. The required condition can be worked out directly at the particle level by making two assumptions. The first one is to assume that in the logarithmic region, the particle velocity components U and V are jointly Gaussian. Such an assumption is reasonably well supported by recent data.[25] Dreeben and Pope[14] report that in their simulation the boundary model preserves the joint-normal velocity PDF; in fact, it was noted by He and Simonin[26] that with analogous boundary conditions (in the context of two-phase particulate flows), the shape of the PDF (any) for incident and reflected particles is preserved. Therefore, one velocity component can be written as a linear function of the other one and of a pure random Gaussian term e:

$$U=\langle U\rangle+\frac{\langle uv\rangle}{\langle v^2\rangle}V+\sqrt{\langle u^2\rangle-\frac{\langle uv\rangle^2}{\langle v^2\rangle}}\,e. \tag{27}$$

The second assumption consists in regarding incoming particles as mirror images of the outgoing ones. The underlying idea is to imagine two mirror ensembles of particles on either side of the boundary $y=y_{\min}$. We then make the assumption that, statistically speaking, the two ensembles are identical in terms of the statistics of fluctuating velocities. This is equivalent to describing the constant-stress region as homogeneous for the Reynolds stresses. Then every time a particle leaves the domain with a normal velocity $V^+_{\rm out}$ there is an equal probability that another particle (the mirror one) starts from the mirror ensemble with a normal velocity $V^+_{\rm in}=-V^+_{\rm out}$. The two longitudinal velocities $U^+_{\rm out}$ and $U^+_{\rm in}$ are linked to the normal ones by the linear relation, Eq. (27), and from the mirror assumption we can identify the two Gaussian random terms of the two mirror particles. This yields the required condition

$$U^+_{\rm in}=U^+_{\rm out}-2\frac{\langle uv\rangle}{\langle v^2\rangle}V^+_{\rm out}. \tag{28}$$

A boundary condition must also be written for the turbulent frequency of the incoming particle. Two formulations can be proposed based on previous ideas. A first possibility is to write directly a relation similar to the one above

$$\omega^+_{\rm int}=\omega^+_{\rm out}-2\frac{\langle v\omega\rangle}{\langle v^2\rangle}V^+_{\rm out}. \tag{29}$$

The derivation developed for the particle velocities would give support to this relation if (V^+,ω^+) was a joint-Gaussian variable. However, there is no reason for (V^+,ω^+) to be Gaussian in the constant-stress region. Although this does not necessarily invalidate the present boundary condition, Eq. (29) has then to be seen as a proposal rather than a consequence of an underlying description. On the other hand, such a boundary condition allows the flux of ω^+, which is $\langle v\omega\rangle$, across the layer to be directly controlled. A second idea is to write the particle boundary condition in terms of $\ln(\omega^+)$ rather than ω^+ itself. Using the variable $\chi^+=\ln(\omega^+/\langle\omega\rangle)$ for the incoming and outgoing particles, the particle boundary condition is now expressed as

$$\chi^+_{\rm in}=\chi^+_{\rm out}-2\frac{\langle v\chi\rangle}{\langle v^2\rangle}V^+_{\rm out}, \tag{30}$$

or for the particle turbulent frequency as

$$\omega^+_{\rm in}=\omega^+_{\rm out}\exp\left(-2\frac{\langle v\chi\rangle}{\langle v^2\rangle}V^+_{\rm out}\right). \tag{31}$$

This second condition may appear more in line with the PDF model used in the present work. Indeed, the stochastic model retained for particle instantaneous frequency rates is based on the log-normal hypothesis and is built so as to yield a joint-Gaussian solution for $(V^+,\ln\omega^+)$ or (V^+,χ^+) in homogeneous turbulence. This does not fully justify the second condition here since the constant-stress region is not homogeneous for the joint variable (V^+,χ^+) and, here again, Gaussianity is only an approximation, though it can be a better one than for (V^+,ω^+). From that Gaussian hypothesis, the correlation $\langle v\chi\rangle$ can be worked out and one finds

$$\langle v\chi\rangle=\frac{\langle v\omega\rangle}{\langle\omega\rangle}, \tag{32}$$

so that it can estimated in the layer from the known expression of $\langle v\omega\rangle$ (see below). This second boundary condition was used by Dreeben and Pope, yet with a different expression for the mean coefficient entering the exponential.[14] However, since a different stochastic model for the particle frequency rate was used (a model yielding a gamma distribution in homogeneous conditions), the reason of ''consistency'' between the stochastic model and the boundary condition is lost. In the particle simulations described below, both conditions Eq. (29) and Eq. (31) have been tested. Both can perform satisfactorily. However, it was found that the second condition was less stable due to the exponential factor, particularly with a small number of particles in the boundary cells. Since both conditions appear as approximations, the first condition was selected since the important correlation $\langle v\omega\rangle$ is controlled throughout the layer in a more direct and efficient way.

To sum up: the detailed conditions for the incoming particle are written in terms of the outgoing one as

$$\begin{aligned}
&y^+_{\rm in}=2y^+_{\rm min}-y^+_{\rm out},\\
&V^+_{\rm in}=-V^+_{\rm out},\\
&U^+_{\rm in}=U^+_{\rm out}-2\frac{\langle uv\rangle}{\langle v^2\rangle}V^+_{\rm out},\\
&\omega^+_{\rm in}=\omega^+_{\rm out}-2\frac{\langle \omega v\rangle}{\langle v^2\rangle}V^+_{\rm out}
\end{aligned} \tag{33}$$

or, alternatively for the last condition (if the boundary condition for the turbulent frequency is chosen to be written in terms of χ^+ instead of ω^+)

$$\chi^+_{\rm in}=\chi^+_{\rm out}-2\frac{\langle \chi v\rangle}{\langle v^2\rangle}V^+_{\rm out}. \tag{34}$$

These conditions are completed with the values for the different correlations.

B. Mean correlations in the logarithmic layer

In the wall-boundary conditions written above, the correlations between the normal velocity and the corresponding variable are given by the theoretical expressions which arise from the equilibrium assumption of the constant-stress region

$$\langle uv\rangle_{th}=-u_*^2,\quad \langle \omega v\rangle_{th}=(C_{\epsilon_2}-C_{\epsilon_1})\frac{u_*}{k_{th}\kappa}\langle\omega\rangle_{th},$$
$$\langle\omega\rangle_{th}=\frac{u_*}{\kappa k_{th} y},\quad k_{th}=\frac{1+3C_0/2}{\sqrt{C_0}}, \tag{35}$$

where $C_0, C_{\epsilon_1}, C_{\epsilon_2}$ are constants of the turbulence model and κ the Von Karman constant. The value of the correlation $\langle v\omega\rangle_{th}$ can be deduced from the transport equation of $\langle\omega\rangle$

$$\frac{\partial\langle v\omega\rangle}{\partial y}=-(C_{\epsilon_2}-C_{\epsilon_1})\langle\omega\rangle^2 \tag{36}$$

and from the variation of $\langle\epsilon\rangle$ in the logarithmic layer. The value of the turbulent kinetic energy normalized by the friction velocity, $k_{th}=k/u_*^2$, is a consequence of the equilibrium assumption and of the particular model considered. This relation, as well as the relations that give the values of the different turbulent intensities ($\langle u^2\rangle, \langle v^2\rangle, \langle w^2\rangle$) can be obtained by manipulating the mean equations. They can also be derived directly from the instantaneous particle equations. In line with the trajectory (or Lagrangian stochastic) point of view which is mainly used in this paper, we develop here this second approach. This further illustrates how SDEs are manipulated and also brings out the assumption already made to obtain the particle boundary conditions. In the constant-stress region, the particle equations for the fluctuating velocities are from Eq. (21):

$$du^+=-v^+\frac{\partial\langle U\rangle}{\partial y}dt-\left(\frac{1}{2}+\frac{3}{4}C_0\right)\frac{\langle\epsilon\rangle}{k}u^+\,dt + \sqrt{C_0\langle\epsilon\rangle}\,dW_u, \tag{37}$$

$$dv^+=-\left(\frac{1}{2}+\frac{3}{4}C_0\right)\frac{\langle\epsilon\rangle}{k}v^+\,dt+\sqrt{C_0\langle\epsilon\rangle}\,dW_v, \tag{38}$$

$$dw^+=-\left(\frac{1}{2}+\frac{3}{4}C_0\right)\frac{\langle\epsilon\rangle}{k}w^+\,dt+\sqrt{C_0\langle\epsilon\rangle}\,dW_w. \tag{39}$$

The assumption of spatial homogeneity for the Reynolds-stress components means now that u^+, v^+, w^+ are stationary stochastic variables. Therefore, mean quantities are constant in time and we have

$$\langle d[(u^+)^2]\rangle=\langle d[(v^+)^2]\rangle=\langle d[(w^+)^2]\rangle=\langle d[u^+v^+]\rangle=0. \tag{40}$$

By applying Ito's rules for diffusion processes, these conditions imply the following relations:

$$-2\langle uv\rangle\frac{\partial\langle U\rangle}{\partial y}-\left(1+\frac{3}{2}C_0\right)\frac{\langle\epsilon\rangle}{k}\langle u^2\rangle+C_0\langle\epsilon\rangle=0, \tag{41}$$

$$-\left(1+\frac{3}{2}C_0\right)\frac{\langle\epsilon\rangle}{k}\langle v^2\rangle+C_0\langle\epsilon\rangle=0, \tag{42}$$

$$-\left(1+\frac{3}{2}C_0\right)\frac{\langle\epsilon\rangle}{k}\langle w^2\rangle+C_0\langle\epsilon\rangle=0, \tag{43}$$

$$-\langle v^2\rangle\frac{\partial\langle U\rangle}{\partial y}-\left(1+\frac{3}{2}C_0\right)\frac{\langle\epsilon\rangle}{k}\langle uv\rangle=0. \tag{44}$$

Consequently, the turbulent intensities are

$$\langle u^2\rangle=k\frac{C_0+2\mathcal{P}/\langle\epsilon\rangle}{1+3C_0/2},\quad \langle v^2\rangle=\langle w^2\rangle=k\frac{C_0}{1+3C_0/2}, \tag{45}$$

and consistency with the definition of k implies that $\mathcal{P}=\langle\epsilon\rangle$, the well-known equilibrium assumption for the constant-stress layer. Then, from Eq. (44), we also have the relation

$$\langle v^2\rangle=\left(1+\frac{3}{2}C_0\right)\frac{\langle uv\rangle^2}{k}, \tag{46}$$

which by equating the two expressions for $\langle v^2\rangle$ yields

$$k=u_*^2\frac{1+3C_0/2}{\sqrt{C_0}}=u_*^2k_{th}. \tag{47}$$

The values of the turbulent intensities which result from the homogeneity assumption and from the particular PDF model used (here the SLM model) are therefore

$$\langle u^2\rangle=u_*^2\frac{C_0+2}{\sqrt{C_0}},\quad \langle v^2\rangle=\langle w^2\rangle=u_*^2\sqrt{C_0}. \tag{48}$$

These equilibrium relations are helpful to check that in the simulations ''correct'' values are obtained. They are also used in the implementation of the particle-boundary conditions. Indeed, the expression of the turbulent kinetic energy k_{th}, which is consistent with the model used, helps to determine the equilibrium values of the fluxes $\langle uv\rangle_f$ and $\langle v\omega\rangle_f$, Eqs. (35). It is these equilibrium or ''fixed'' values (referred to with the index f) that are used in the particle boundary conditions, Eqs. (33).

C. Conditions for averaged variables

The wall-boundary conditions ensure that ensemble averages over the particles that cross the domain boundary, denoted by $\langle\cdot\rangle_b$, satisfy the conditions:

$$\begin{aligned}&\langle v_{\rm in}\rangle_b=-\langle v_{\rm out}\rangle_b,\\ &\langle u_{\rm in}\rangle_b=-\langle u_{\rm out}\rangle_b,\\ &\langle v_{\rm in}^2\rangle_b=\langle v_{\rm out}^2\rangle_b,\\ &\langle u_{\rm in}^2\rangle_b=\langle u_{\rm out}^2\rangle_b,\\ &\langle u_{\rm in}v_{\rm in}\rangle_b=\langle u_{\rm out}v_{\rm out}\rangle_b.\end{aligned} \tag{49}$$

Furthermore, the precise value of the different fluxes can be worked out from the knowledge of the (Eulerian) PDF in the vicinity of the boundary noted $f_b(\mathcal{U},\mathcal{V})$. Indeed, the mean value of any function $Q(U,V)$ over the particles crossing the domain boundary, $\langle Q\rangle_b$, which represent the flux of Q is given by

$$\langle Q\rangle_b=\frac{1}{C}\int_0^\infty\left(\int_{-\infty}^\infty Q(\mathcal{U},\mathcal{V})f_b(\mathcal{U},\mathcal{V})d\mathcal{U}\right)\mathcal{V}\,d\mathcal{V} \tag{50}$$

where the normalization constant

$$C=\int_0^\infty\left(\int_{-\infty}^\infty f_b(\mathcal{U},\mathcal{V})d\mathcal{U}\right)\mathcal{V}\,d\mathcal{V} \tag{51}$$

is in fact the number n_b of incoming and outcoming particles crossing a unit of boundary surface per second, with $n_{\rm out}=n_{\rm in}=n_b$. Supposing that $f_b(\mathcal{U},\mathcal{V})$ is a joint-normal PDF $\mathcal{N}(\langle U\rangle,0,\sigma_u,\sigma_v,r_{uv})$, with $r_{uv}=\langle uv\rangle/(\sigma_u\sigma_v)$, we obtain

$$\begin{aligned}
&n_b=\frac{\sigma_v}{\sqrt{2\pi}},\\
&\langle u_{\rm out}\rangle_b=-\tfrac{1}{2}\sqrt{2\pi}r_{uv}\sigma_u,\\
&\langle v_{\rm out}\rangle_b=-\tfrac{1}{2}\sqrt{2\pi}\sigma_v,\\
&\langle u_{\rm out}^2\rangle_b=(1+r_{uv}^2)\sigma_u^2,\\
&\langle v_{\rm out}^2\rangle_b=2\sigma_v^2,\\
&\langle u_{\rm out}v_{\rm out}\rangle_b=2r_{uv}\sigma_u\sigma_v.
\end{aligned} \tag{52}$$

The relations between the different ensemble averages over the incoming and the outcoming particles, Eqs. (49), are then deduced by applying the operator $\langle\cdot\rangle_b$ to the wall-boundary conditions and by using the previous expressions, Eqs. (52). It is therefore seen that no energy is added when the incoming particles follow the wall-boundary conditions and that the resulting effect on the turbulent intensities $(\langle u^2\rangle,\langle v^2\rangle,\langle w^2\rangle)$ is a Neumann condition. A similar conclusion could be reached for the shear stress $\langle uv\rangle$. However, in practice the wall-boundary conditions are applied using the fixed or ''theoretical'' expressions of the equilibrium layer for the correlations $\langle uv\rangle_f$ and $\langle v\omega\rangle_f$, Eqs. (35), as already mentioned above. This amounts in fact to giving to the fluxes a fixed value and the resulting effect for the calculated correlations $\langle uv\rangle$ and $\langle u\omega\rangle$ in the boundary cells is a Dirichlet condition.

D. Simulation of a constant-stress layer

The boundary conditions developed above are written for the instantaneous values of the particle variables along the spirit of the method. Once they are expressed, all the different boundary conditions for every moment of the velocity or the frequency can be derived and one must obtain all the correct mean statistics of the constant-stress region from these two relations. This was assessed by simulating one segment of a constant-stress layer and checking, once the particle boundary conditions are used, that various statistics are correctly reproduced. The complete algorithm was used, although significant simplifications can be made: with mean pressure assumed constant throughout the layer, it becomes basically a 1D calculation in which particles are moved only in the normal direction. The friction velocity u_* was given a fixed value and, from the previous boundary conditions, this amounts to setting $\langle uv\rangle=-u_*^2$. We have placed the upper boundary of the layer in the constant-stress region and applied there the same limit conditions as for the other boundary close to the wall.

TABLE I. Results for the constant-stress region of the turbulent boundary layer; u_*, friction velocity.

Statistics	Present work	Pope (1991)	Experiment
k/u_*^2	3.35	3.4	3.8
$\langle u^2\rangle/u_*^2$	2.90	2.99	4.3
$\langle v^2\rangle/u_*^2$	1.90	1.96	1.0
$\langle w^2\rangle/u_*^2$	1.90	1.96	2.4

The simulation was performed to check the validity of the particle boundary conditions and also to determine the value of the constant $C_{\epsilon 1}$ of the model. Other constants are first given the following values $C_{\epsilon 2}=1.9$, $\sigma^2=1$ and $C_0=3.5$. That leaves two unknown constants in the model, namely C_χ and $C_{\epsilon 1}$. Actually, these two constants are dependent and one can be found as a function of the other one to obtain satisfactory results in the logarithmic region. Indeed, it is seen from the model equation for particle frequency rate, Eq. (9), that the constant C_χ controls the level of the correlation with the normal velocity $\langle v\omega\rangle$, or in other words turbulent diffusion across the layer. At equilibrium, one must have the balance

$$\frac{\partial\langle v\omega\rangle}{\partial y}=-S_\omega^{\rm eq}\langle\omega\rangle^2 \tag{53}$$

with $S_\omega^{\rm eq}=C_{\epsilon 2}-C_{\epsilon 1}$. Thus, for a fixed value of C_χ, simulations are performed and the value of $C_{\epsilon 1}$ is tuned to obtain the correct profiles of the different mean quantities and the correct value of the Von Karman constant $\kappa=0.41$. At equilibrium, this correct value is obtained indifferently from the profiles of $\partial\langle U\rangle/\partial y$ or $\langle\omega\rangle$. For the value $C_\chi=5$ which was retained, the constant $C_{\epsilon 1}$ is then determined to be $C_{\epsilon 1}=1.35$.

The results of computation are presented in Table I and compared to the experimental data.[18] They are expected to be the same as the results of Pope[18] and differences are supposedly due to the statistical noise. The values obtained for the velocity component turbulent intensities reflect the particular model that was used (SLM), Eqs. (48), and the value of the constant $C_0(C_0=3.5)$. Different equilibrium values can be obtained for these intensities by using a different model, for example a particle-based IPM model.[22] It must be stressed here that the whole procedure has to be performed again if one is to use a different value of C_χ (for example, assuming $C_\chi=1.6$ requires $C_{\epsilon 1}=1.15$) or if one uses a different PDF model.

IV. NUMERICAL APPROACH

Although particle methods are basically grid-free (see vortex methods or smooth particle hydrodynamics), the present numerical approach is an example of a particle/mesh method. The computational domain is divided into a number of cells (whose structured or unstructured nature does not matter) and averaged quantities such as mean velocity components $\langle U_i \rangle$ are simply obtained as local ensemble means.

In a general case of compressible flows, pressure is included in the state vector; in the PDF method, it is governed by its own evolution equation, as recently proposed by Delarue and Pope.[27] In a particle method for incompressible flows, considered here, the specific difficulty of the mean pressure-gradient calculation is related to the satisfaction of the continuity equation. This implies two requirements: at the end of each time step, the particle concentration must be uniform and at the same time the mean velocity field must be of zero divergence. For some particular flows, an easy estimation can be found that satisfies both constraints. This was the case of a mixing layer computation where a pseudo-1D approach was used and where the estimation of the mean pressure-gradient is less difficult than in the general case.[7] However, a general procedure is of course more desirable. We present here a general numerical scheme (2D/3D) which is a fractional time step method implemented in a PDF code developed by the authors. The idea is to satisfy the two constraints separately by considering one variable independently from the other (particle location first and then particle velocity).

At every time step, the following are performed:

Step 1. Integration of the evolution equations for particle velocity and dissipation rate while particle locations are left unchanged. Second-order numerical schemes are used for the SDE that yield $\tilde{\mathbf{U}}^+(t_{n+1})$ and $\omega^+(t_{n+1})$; variance reduction techniques (VRT) are applied at the same time. The main aim of using VRT is to reduce the statistical error of the solution, either by generating new samples of random numbers (so-called tetrahedral sampling) or by solving additional equations for the chosen moments of the solution to reduce the fluctuations in the coefficients of the SDE for particle evolution.[28]

Step 2. Particles are now moved. After this convection step, the concentration or mean particle density $\tilde{\rho}$ is calculated. A potential field is deduced from the Poisson equation[1]

$$\nabla^2 P_1 = \frac{2}{(\Delta t)^2}\left(1-\frac{\tilde{\rho}}{\rho_0}\right) \tag{54}$$

with homogeneous Neumann boundary conditions; particle locations are then corrected to enforce a uniform particle concentration ρ_0:

$$\mathbf{x}^+(t_{n+1}) = \mathbf{x}^+(t_n) + \frac{\Delta t}{2}(\mathbf{U}^+(t_n) + \tilde{\mathbf{U}}^+(t_{n+1})) - \frac{1}{2}(\Delta t)^2 \nabla P_1. \tag{55}$$

Step 3. Boundary conditions (33) are applied. To do so, the friction velocity u_* is determined locally in each boundary cell by assuming that the mean velocity $\langle U \rangle$ is also in the logarithmic region. This friction velocity is worked out from a fixed point calculation and is based on the mean velocity computed at the beginning of the time step (or the end of the previous iteration, see step 5). If we write $\langle U \rangle(x_c, y_c)$ for the mean longitudinal velocity in a boundary cell whose center has the coordinates (x_c, y_c), the friction velocity $u_*(x_c)$ that will be used for the particle crossing the lower cell boundary is obtained from

$$\frac{\langle U \rangle(x_c, y_c)}{u_*(x_c)} = C + \frac{1}{\kappa}\ln\left(\frac{y_c u_*(x_c)}{\nu}\right), \tag{56}$$

where the constant C is $C = 3.35$.

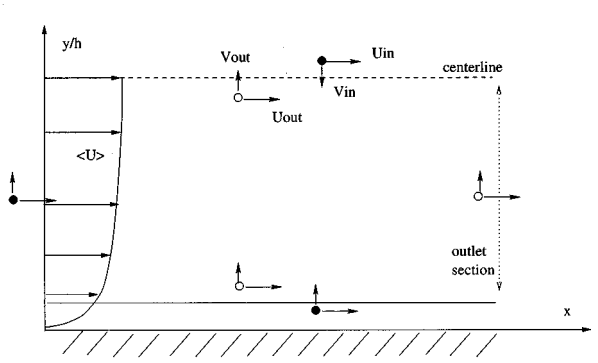

FIG. 2. Sketch of the turbulent channel flow. Boundary sections are indicated and typical particle velocity boundary conditions are represented.

Step 4. The mean velocity field $\langle \tilde{U} \rangle$ is computed in each cell. A mean pressure-gradient is calculated from another Poisson equation

$$\nabla^2 P_2 = \frac{1}{\Delta t}\nabla \langle \tilde{\mathbf{U}} \rangle \tag{57}$$

with homogeneous Neumann boundary conditions at the wall and at the symmetry line; the computed pressure gradient is used to modify particle velocities

$$\mathbf{U}^+(t_{n+1}) = \tilde{\mathbf{U}}^+(t_{n+1}) - (\Delta t)\nabla P_2, \tag{58}$$

so that the mean velocity field satisfies the continuity equation. At this step, a condition that drives the flow is imposed. Generally, it is done by specifying the velocity profile at the inlet; the outlet condition is assumed for pressure (constant derivative of the mean pressure in the streamwise direction). Alternatively (and this was also tested in the computations), periodic boundary conditions can be used for a fully developed channel flow; in this case, pressure difference between inlet and outlet is imposed.

Step 5. Moments are computed locally by ensemble averaging over all particles in a given cell.

V. TURBULENT CHANNEL FLOW

A turbulent channel flow was then simulated. This is a flow with a simple geometry (Fig. 2) but with all the desired

characteristics to test the boundary conditions as well as the general algorithm.

The fully developed turbulent channel flow has received a great deal of attention, both experimentally[15,29,30,25] and numerically.[31] Numerical simulations provide complete data sets and access to quantities often unavailable to measurements. Such a data set, obtained by DNS was used by Dreeben and Pope[14] when they reported channel flow results. However, in the present work, the experimental data set of Comte-Bellot[15] was selected as the reference data against which the model its and numerical performance will be assessed. First of all, this choice is made to complement results already presented by Dreeben and Pope since a different channel flow is considered. Secondly, the experiments of Comte-Bellot correspond to the highest Reynolds numbers reported (from 57 000 to 230 000, based on the centerline velocity) while direct numerical simulations were only performed at low Reynolds numbers[31] (3300 and 7900). Low-Reynolds effects are known to affect turbulent intensities[29,30,25] and their distribution across the wall boundary layer. This may be of some significance for the present model. The justification for the particle wall-boundary conditions proposed above relies on a description where turbulent intensities are roughly constant at least in the constant-stress layer. This is only found true at very high-Reynolds numbers, in particular for the streamwise fluctuating velocity and at slightly lower Reynolds numbers for the normal component (Ref. 29, Figs. 3 and 4). Consequently, it is hoped that the wall conditions and also the form of the model which is used are on somewhat safer grounds at very-high number flows.

The experiments of Comte-Bellot[15] were carried out with a channel half-width of $h=0.09m$. Measurements were made for three Reynolds numbers, $Re=57\,000$, 120 000, and 230 000, based on the channel half-width and the bulk velocity; extensive data, including many higher-order statistics such as two-point correlations, energy spectra, skewness and flatness factors, were reported. For the intermediate Reynolds number ($Re=120\,000$), measurements were performed at a number of longitudinal distances from the inlet to assess whether the flow had reached its fully developed state. Experimental profiles revealed that a distance of at least $x/h\sim100$ was necessary for the different statistics (particularly high-order ones) to reach their limit value and the values reported were taken at $x/h=118$. For this Reynolds number, the centerline velocity was 22.2 m/s and the friction velocity was measured as $u_*=0.8$ m/s. Based on this friction velocity, the Reynolds number is therefore $Re_\tau=4800$. The measurements indicate that the different velocity moments, made nondimensional with wall units, are not sensitive to the Reynolds number (with the exception of the longitudinal skewness factor but only in the central region of the channel). This supports the idea that, in that range of Reynolds numbers, the friction velocity u_* is the relevant scaling parameter. In the near-wall region, measurements of the moments of the streamwise fluctuating velocity confirm that, for this high-Reynolds number flow, statistics of the fluctuating velocities are now nearly constant, roughly in line with the homogeneous assumption for these variable. The same measurements also show a departure from Gaussianity for the streamwise fluctuating velocity, which remains moderate in the logarithmic region (the skewness and flatness factors are $S_u\sim-0.1$ and $F_u\sim2.8$).

Calculations have been performed for conditions corresponding to the intermediate Reynolds number of the experiment, $Re=120\,000$. Due to homogeneity in the longitudinal direction, the channel flow can actually be simulated with a 1D approach. However, a full 2D calculation was performed to test the code, to illustrate how the method works in general and also to investigate some numerical issues. Particles are first initialized with a uniform concentration and with respect to given initial fields. At the outlet, particles leaving the domain are replaced at the inlet of the computed section. This corresponds to periodic conditions and implies that particles are marched to an homogeneous solution (in the longitudinal direction). For particles leaving through the channel centerline boundary (only a half-channel is simulated), simple symmetry conditions are applied

$$V_{\rm in}^+=-V_{\rm out}^+,\qquad U_{\rm in}^+=U_{\rm out}^+,\qquad \omega_{\rm in}^+=\omega_{\rm out}^+. \tag{59}$$

For the other boundary, the former conditions, Eqs. (33) remain valid; they are placed in the constant-stress region of the boundary layer. The locations of the center of the boundary cells and of the boundary surface $y_{\rm min}$ are defined at the beginning of the calculation. The center of the boundary cells, $yc_{\rm min}$ is taken as $0.05\times h$. The value of $y_{\rm min}$ is then determined by the number of cells in the normal direction. For a number of 25 cells, as used typically, this gives $y_{\rm min}=0.03\times h$. In wall units, using the experimental value of the friction velocity as an indication, $u_*=0.8$ m/s, this means that we have $y_{\rm min}^+=144$ and $yc_{\rm min}^+=240$. Both distances satisfy the two constraints $y^+\geqslant30$ and $y/h\leqslant0.1$ and are well within the logarithmic layer.

First of all, it must be checked that a fully developed state is indeed reached in the simulations. This implies that after some necessary time for turbulence development, various statistical quantities reach a steady state. One such verification is shown in Fig. 3 which represents the time evolution of the streamwise and normal turbulent intensities as well as the shear stress normalized by the friction velocity. The quantities plotted in Fig. 3 actually represent the ''y-averaged'' values of these variables across the channel (spatial averaging in the y direction) and are taken at the outlet section. Since turbulent quantities are not homogeneous across the channel, the actual numbers obtained for the different intensities are meaningless. They are just regarded here as indicators used to assess whether a steady state is found. It is seen from the time evolutions of these ''y-averaged'' mean values, that after a time lag of about $\Delta t\simeq0.3$ s such a steady state is indeed reached. Using a bulk velocity of about $U_b\sim20$ m/s, this corresponds to a longitudinal distance of around $x/h\sim70$ which is in line with the required experimental distance (the exact figures depend of course on how particles are initialized). After this transient

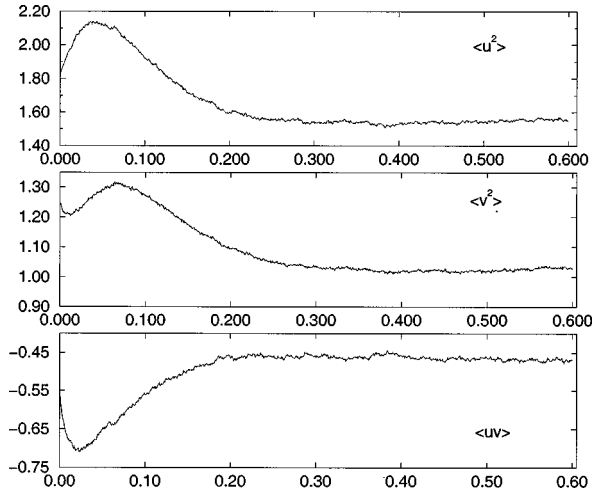

FIG. 3. Evolution of the computed $\langle u^2 \rangle$, $\langle v^2 \rangle$, and $\langle uv \rangle$ (averaged across a section) as a function of time.

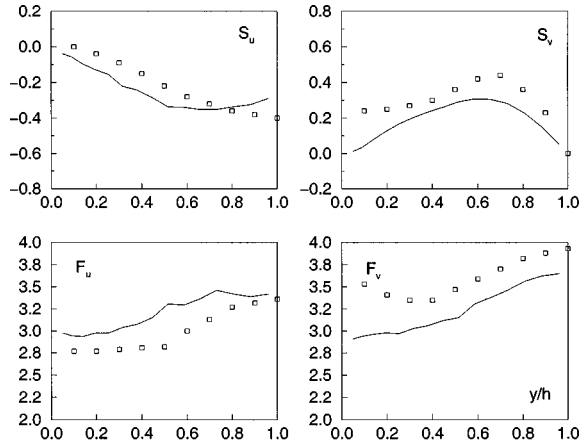

FIG. 5. Skewness and flatness factors of the streamwise and the cross-stream velocity components as a function of the normalized wall distance. Comparison of the computation (solid line) with the experiment of Comte-Bellot (□).

period, the mean quantities which are obtained at the end of each time step as ensemble averages performed on the particles present at that time in the given cell, are also averaged in time (this time averaging basically reduces the level of statistical noise due to the finite number of particles). The results displayed below have been obtained by time-averaging the ensemble means using 150 time steps, which represents a time interval of about 0.10 s. Here also, different time-averaged results have been compared for successive time intervals to check that identical results are obtained. Time averaging was only performed for visualization purposes but was not applied during the calculation. In the simulation, only the ensemble averages were used in the particle governing equations.

The plots shown in Fig. 4 present mean streamwise velocity as well as second-order statistics, i.e., components of the Reynolds-stress tensor R_{ij} and the turbulent kinetic energy as functions of the cross-stream coordinate normalized by the channel half-width. The computation results are compared with the experimental data of Comte-Bellot[15] obtained for $Re_\tau = 4800$ (based on the friction velocity) and the recent DNS data of Mansour (as referenced by Dreeben and Pope[14]) obtained for the moderate Reynolds number, $Re_\tau = 395$. For reasons mentioned above, it is rather with the former data set that the outcome of the presented PDF method should be compared. The calculated value of the friction velocity, u_*, is about 0.84 m/s when the stationary regime is reached, compared with 0.8 m/s in the experiment. It is noticed that the shear stress R_{12} and the turbulent kinetic energy k are in satisfactory agreement with experiment. On the other hand, a discrepancy in the distribution of this energy between the diagonal components of the Reynolds-stress tensor is observed. The numerical values obtained at the wall boundaries reflect the model predictions of a turbulent boundary layer for the SLM model as explained in Sec. III D. Contrary to the experimental evidence, the transverse and the spanwise components of the Reynolds-stress tensor are predicted to be equal. This is an inherent feature of the model used here and the distribution of turbulent kinetic energy over the components ($\langle u^2 \rangle$, $\langle v^2 \rangle$, and $\langle w^2 \rangle$ values) can possibly be improved by going to more evolved PDF models.

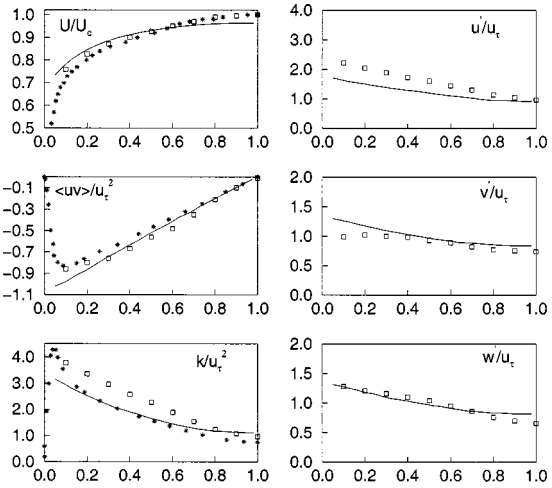

FIG. 4. Streamwise mean velocity, shear stress, kinetic energy and fluctuating velocities plotted as a function of the normalized cross-stream coordinate. Comparison of the computation (solid line) with the experiment of Comte-Bellot (□) and DNS results (⋆).

To illustrate the capacities of the PDF approach, higher-order statistics, unavailable in the RSM closures, have also been computed. They are skewness S and flatness F of velocity components. As shown in Fig. 5, qualitative agreement with experimental data is satisfying. In spite of the simplicity of the model, the correct levels and trends are found across the channel.

It is worth recalling that present results have been obtained with the simplest PDF model (the simplified Langevin model for particle velocity) and with the standard form of the model. It seems likely that other form of the matrix G_{ij} would improve second-order velocity results. Experience with the simulations reveals also that the numerical predictions are sensitive to the behavior of $\langle \omega \rangle$ near the center line.[14] However, no special tuning or particular modification of terms appearing in the model equations was attempted

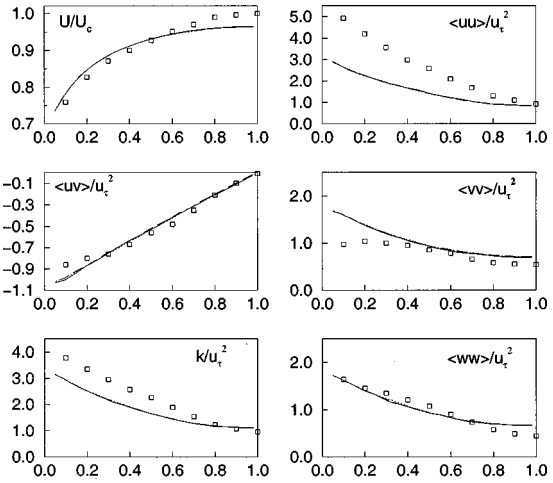

FIG. 6. Streamwise mean velocity, shear stress, and Reynolds-stress tensor components plotted as a function of the normalized cross-stream coordinate and calculated for different number of particles per cell (npc). Solid line (npc=100), dotted line (npc=150) and long dashed line (npc=200).

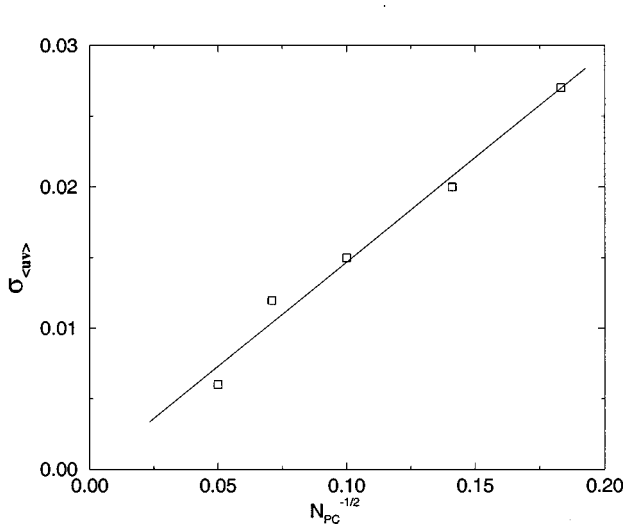

FIG. 7. Standard statistical error for one of computed statistics (shear stress $\langle uv \rangle$) vs number of particles per cell N_{pc}. Line is least-square estimate.

here. Indeed, one of the purposes of the channel flow case was also to explore some numerical issues that may remain relevant for other cases. Once properly implemented, this is a simple case easy to run with 10 000 to 100 000 particles on a workstation at relatively low computational requirements. As an example, results of the computation discussed above were performed with 25 000 particles on 10×25 grid to attain a reasonable trade-off between the computational cost and the statistical noise level. On a HP 9000/735 machine, it takes typically a few CPU minutes (about 20 min for 1000 time steps) to achieve convergence towards the steady state for the above parameters. The sensitivity to the various parameters of the numerical calculation was analyzed. Independence with respect to the time step was checked and seen to be obtained, even with time steps that are not too dramatically low, when high-order numerical schemes are used (higher order than the simple Euler scheme, at least). However, details on numerical schemes for SDEs are outside the scope of this paper and we concentrate on the sensitivity with respect to the number of particle per cell. This is an important issue for practical simulations. The present method is a Monte Carlo method and is known to converge at a rate that scales as $N^{1/2}$ with the number of particles N. Since computational requirements increase nearly linearly with N, it is important to see whether satisfactory answers can be obtained with a number of particles as low as possible.

In Fig. 6, time-averaged mean results are shown for different numbers of particles per cell (note that in this figure turbulent intensities rather than the fluctuating velocities are plotted since this magnifies any difference and that the scale for the mean longitudinal velocity has been changed). This figure gives only qualitative information, but suggests that small bias seems to be encountered and that satisfactory results can be obtained with a reasonable number of particles per cell (actually, results obtained with 50 particles per cell already give answers which are very close to the limit ones when $N\rightarrow\infty$). According to Pope,[28] the overall error of the PDF computation can be separated into a statistical and deterministic part, the latter involving bias, spatial and temporal discretization errors. It is the former, i.e., the statistical error due to the finite number of stochastic particles used in the simulation that we will consider now. In order to measure the statistical error related to varying number of particles per cell (N_{pc}), we computed this error out of the y-averaged values of some variables recorded after the stationary state has been achieved. The results are plotted in Fig. 7; it is clearly seen that the error varies indeed as $N_{pc}^{-1/2}$.

Lastly, the importance of variance reduction techniques (VRT) is illustrated in Fig. 8. The two curves represent the same ''y-averaged mean intensities'' as a function of time. They are obtained with the same number of particles, in that case only 30 particles per cell. However, in the first one

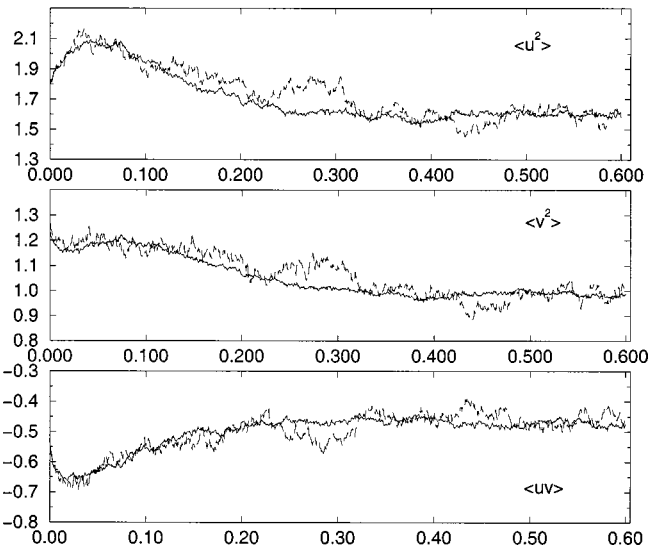

FIG. 8. Evolution of the computed $\langle u^2 \rangle$, $\langle v^2 \rangle$, and $\langle uv \rangle$ (averaged across a section) as a function of time. The solid line represents results obtained when VRT (variance reduction technique) is on, while the dashed line represents results when VRT is off. Both curves are obtained with the same number of particle per cell, $N_{pc}=30$.

TABLE II. Qualitative assessment of the variance reduction techniques: relative statistical error for chosen variables and the CPU time.

	No VRT	VRT for ω	VRT for **U**	VRT for both
$\langle U \rangle$	1.00	1.04	0.89	0.86
$\langle u^2 \rangle$	1.00	0.76	0.33	0.46
$\langle v^2 \rangle$	1.00	0.89	0.39	0.38
$\langle \omega \rangle$	1.00	0.25	0.85	0.23
Relative CPU	1.00	1.07	1.66	1.63

variance reduction techniques are off while in the second one they are applied. It is clear that the second curve fluctuates far less than the first one. The reduction in the statistical error for mean quantities which are calculated with a finite number of particles is striking. To obtain such a result without VRT would have required using a many more particles. Thus, for a given acceptable precision, these techniques allow simulations to be performed with less particles therefore reducing computational requirements. A quantitative assessment of the performance of the VRT is presented in Table II. A relative CPU cost of computations without VRT, with VRT for either velocity or turbulent frequency only, and, at last, for the two variables is gathered there together with the relative statistical error in chosen variables recorded once the stationary solution has been achieved. It is clearly seen that VRT applied to the turbulent frequency affects heavily this variable but much less Reynolds-stress components. On the other hand, VRT applied to velocity moments helps reducing statistical error in these variables but has practically no influence on the turbulent frequency. For both kind of VRT applied, statistical error in mean velocity varies only slightly. Finally, the variance reduction technique used here requires the calculation of statistics on $4 \times N_{pc}$ supplementary particles in each cell.[28] The reported costs have been obtained on a sequential machine. Yet, the method has the potential to be parallelized during step 1, which should subsequently reduce the computational costs associated with the variance reduction technique.

VI. CONCLUSION

The model applied in this work represents a closure for the joint velocity-dissipation (or velocity-frequency) PDF equation. The model can be seen as a Lagrangian stochastic approach since it consists in simulating a large number of particles. At present, the vector of the state variables attached to each particle includes location, velocity, and frequency. These stochastic particles try to mimic the behavior of real fluid particles and aim at simulating the statistics of the flow.

In this paper, wall-boundary conditions developed in terms of the particle instantaneous properties have been proposed. They reproduce all the known statistics of the logarithmic layer and correspond to wall functions in the PDF context. Apart from the condition used for the particle frequency rate, the wall boundary conditions are similar to the ones proposed by Dreeben and Pope. However, a new derivation has been put forward. A general pressure gradient algorithm has also been implemented in a particle code to ensure that the mean continuity equation is satisfied at each step of the particle simulation. Both developments allow wall-bounded nonhomogeneous turbulent flows to be computed with a full 2D/3D PDF standalone approach. This was demonstrated for the case of a high-Reynolds number channel flow. The purpose of that simulation was not to exhibit the best possible results that one can get with a PDF approach, but rather to validate the wall-boundary conditions and to illustrate how the method works with the simplest PDF model (SLM). With respect to that objective, comparison with experimental data, which includes skewness and flatness factors, is satisfactory.

Current developments of this work aim at improving computational efficiency (variance reduction techniques, more efficient numerical schemes for SDEs) and at introducing numerical models to inert and/or reactive variables. To extend PDF description of turbulent flows, length scale information should be included. This could be done by adding some variables, or by coupling PDF method to SPH where particles would provide ''sub-kernel'' information.

[1] S. B. Pope, ''PDF methods for turbulent reactive flows,'' Prog. Energy Combust. Sci. **11**, 119 (1985).
[2] S. B. Pope, ''Lagrangian PDF methods for turbulent flows,'' Annu. Rev. Fluid Mech. **26**, 23 (1994).
[3] J.-P. Minier, ''Lagrangian stochastic modelling of turbulent flows,'' *Advances in Turbulence Modelling, 1997–1998 Lecture Series Programme* (Von Karman Institute, Rhode-Saint-Genese, 1998).
[4] P. J. Colluci, F. A. Jaberi, P. Givi, and S. B. Pope, ''The filtered density function for large-eddy simulation of turbulent reactive flows,'' Phys. Fluids **10**, 499 (1998).
[5] R. O. Fox, ''Computational Methods for Turbulent Reacting Flows in the Chemical Process Industry,'' Revue de l'Institut Français du Pétrole, Vol. 51, No. 2, 1996.
[6] J. Pozorski and J.-P. Minier, ''PDF modeling of dispersed two-phase turbulent flows,'' Phys. Rev. E **59**, 855 (1999).
[7] J.-P. Minier and J. Pozorski, ''Analysis of a PDF model in a mixing layer case,'' *10th Symposium on Turbulent Shear Flows* (The Pennsylvania State University, University Park, PA, 1995), p. 26.
[8] T. S. Lundgren, ''Distribution functions in the statistical theory of turbulence,'' Phys. Fluids **10**, 969 (1967).
[9] T. D. Dreeben and S. B. Pope, ''PDF and Reynolds-stress modelling of near-wall turbulent flows,'' Phys. Fluids **9**, 154 (1997).
[10] T. D. Dreeben and S. B. Pope, ''Probability density function/Monte Carlo simulation of near-wall turbulent flows,'' J. Fluid Mech. **357**, 141 (1998).
[11] P. E. Kloeden and E. Platen, *Numerical Solution of Stochastic Differential Equations* (Springer-Verlag, Berlin, 1992).
[12] J. P. Minier and D. Talay (in preparation).
[13] M. S. Anand, S. B. Pope, and H. C. Mongia, ''A PDF method for turbulent recirculating flows,'' *Turbulent Reactive Flows, Lecture Notes in Engineering* (Springer-Verlag, 1989), pp. 672–693.
[14] T. D. Dreeben and S. B. Pope, ''Wall-function treatment in PDF methods for turbulent flows,'' Phys. Fluids **9**, 2692 (1997).
[15] G. Comte-Bellot, *Ecoulement Turbulent Entre Deux Parois Paralleles* (Publ. Scientifiques et Techniques du Ministère de l'Air, Paris, 1965).
[16] D. C. Haworth and S. B. Pope, ''A generalized Langevin model for turbulent flows,'' Phys. Fluids **29**, 387 (1986).
[17] S. B. Pope and Y. L. Chen, ''The velocity-dissipation probability density function model for turbulent flows,'' Phys. Fluids A **2**, 1437 (1990).
[18] S. B. Pope, ''Application of the velocity-dissipation probability density function model to inhomogeneous turbulent flows,'' Phys. Fluids A **3**, 1947 (1991).
[19] L. Arnold, *Stochastic Differential Equations: Theory and Applications* (Wiley, New York, 1974).
[20] C. W. Gardiner, *Handbook of Stochastic Methods for Physics, Chemistry and the Natural Sciences*, corrected 2nd ed. (Springer-Verlag, Berlin, 1990).

[21]J. P. Minier and J. Pozorski, ''Derivation of a PDF model for turbulent flows based on principles from statistical physics,'' Phys. Fluids **9**, 1748 (1997).
[22]S. B. Pope, ''On the relationship between stochastic Lagrangian models of turbulence and second-moment closures,'' Phys. Fluids **6**, 973 (1994).
[23]P. R. Van Slooten, Jayesh, and S. B. Pope, ''Advances in PDF modeling for inhomogeneous turbulent flows,'' Phys. Fluids **10**, 246 (1998).
[24]A. S. Monin and A. M. Yaglom, *Statistical Fluid Mechanics* (MIT Press, Cambridge, MA, 1971).
[25]F. Durst, J. Jovanovic, and J. Sender, ''LDA measurements in the near-wall region of a turbulent pipe flow,'' J. Fluid Mech. **295**, 305 (1995).
[26]J. He and O. Simonin, ''Numerical modelling of dilute gas-solid turbulent flows in vertical channel,'' Electricité de France Report No. 95NB00009, Chatou, 1995.
[27]B. Delarue and S. B. Pope, ''Application of PDF methods to compressible turbulent flows,'' Phys. Fluids **9**, 2704 (1997).
[28]S. B. Pope, ''Particle method for turbulent flows: Integration of stochastic model equations,'' J. Comput. Phys. **117**, 332 (1995).
[29]T. Wei and W. W. Willmarth, ''Reynolds number effects on the structure of a turbulent channel flow,'' J. Fluid Mech. **204**, 57 (1989).
[30]R. A. Antonia, M. Teitel, J. Kim, and L. W. B. Browne, ''Low-Reynolds effects in a fully developed turbulent flow,'' J. Fluid Mech. **236**, 579 (1992).
[31]J. Kim, P. Moin, and R. Moser, ''Turbulence statistics in fully developed channel flow at low Reynolds number,'' J. Fluid Mech. **177**, 133 (1987).